

Loop effect in the detection of neutrinophilic dark matter model with a spin-0 mediator

Tong Li^{1,*} and Jiajun Liao^{2,†}

¹*School of Physics, Nankai University, Tianjin 300071, China*

²*School of Physics, Sun Yat-Sen University, Guangzhou 510275, China*

Abstract

A connection between the neutrinos and the dark matter (DM) candidate is described in the neutrinophilic DM model. In this model the DM particle and neutrinos can convert into each other and thus the interaction leads to novel recoil spectrum in both the DM direct detection experiments and neutrino scattering experiments. We study the detection of neutrinophilic DM by evaluating both the tree-level and loop-level contributions to the coherent elastic neutrino-nucleus scattering and the DM direct detection. We illustrate the detection by taking the framework of a simplified neutrinophilic DM model with a Dirac fermionic DM χ and a spin-0 mediator. For the CP phase in the quark sector being 0 and $\pi/2$, the detection processes are dominated by the tree-level and loop-level contribution, respectively. We investigate the constraints on the couplings between the mediator and the DM particle or the quarks by fitting to the COHERENT data. The parameter space with m_χ larger than the maximal energy of incoming neutrinos can be also constrained by including the loop-level contribution. The DM absorption from the tree-level contribution is sensitive to the sub-GeV DM and the elastic DM-nucleus scattering induced by loop diagrams can probe the DM with several tens of GeV mass in future DM direct detection experiments.

arXiv:2008.00743v1 [hep-ph] 3 Aug 2020

* litong@nankai.edu.cn

† liaojiajun@mail.sysu.edu.cn

I. INTRODUCTION

The existence of dark matter (DM) has been established by abundant cosmological and astrophysical observations. Apart from the gravitational effects originating from the DM in the large scale, the microscopic nature of DM particles still remains unknown. The DM direct detection (DD) looks for the DM scattering off the nucleus target materials and may reveal the DM characteristics as elementary particle beyond the Standard Model (SM). On the other hand, the nature of neutrinos is most analogous to that of DM in the SM and the neutrino flavor change in oscillations indicates the only BSM physics observed in the laboratory so far. It is thus natural to expect that there exists a connection between neutrinos and DM particle and one can unveil new physics from the strong complementarity among different facilities of neutrino and DM DD experiments.

The so-called neutrinophilic DM model describes a hypothesis in which the DM particle (denoted by χ) only interacts with neutrinos [1–11]. This DM candidate can be realized as sterile neutrinos (see a recent review Ref. [12] and references therein), a supersymmetric neutralino annihilating into neutrinos via a sneutrino mediator [1], the lightest right-handed sneutrino [13] or in the Majoron-like model with a light pseudoscalar boson [14–16]. The advantage of this model is that the DM particle and neutrinos can convert into each other and thus the interaction can lead to novel recoil spectrum in both DM DD experiments and neutrino scattering experiments. Recently, different groups studied the conversion to an exotic fermion which could be a DM particle in the coherent elastic neutrino-nucleus scattering ($\text{CE}\nu\text{NS}$) [17–20]. Also, given the reversed process with an incoming χ and an emitted neutrino, Refs. [21] and [22] proposed the DD signature from the absorption of fermionic DM to search for sub-GeV DM with vector interaction. Ref. [20] studied the case of scalar interaction for DM absorption.

For the studies of DM-neutrino interaction in Ref. [20], the authors assumed that the interaction is mediated by a scalar field a via the Yukawa couplings $g_\chi \bar{\chi} \nu a + g_q \bar{q} q a$. The pseudoscalar quark current $\bar{q} i \gamma_5 q$ however leads to effective coupling for nuclear spin-dependent (SD) interaction which is determined by a sum over spin-up and spin-down nucleons with opposite signs [23] and is thus neglected for heavy CsI nuclei in COHERENT experiment [24]. Analogously, in the DM DD experiment, the corresponding tree-level DM-quark contact interaction through a pseudoscalar mediator can also result in a momentum-suppressed SD scattering cross section and thus an undetectable event rate. In contrast, it is worth emphasizing that the tree-level interactions induced by pseudoscalar quark current can generate loop diagrams which in turn give scalar interactions and non-momentum-suppressed spin-independent (SI) scattering. This loop effect has been taken into account in both simplified frameworks and UV complete models for detecting the Weakly Interacting Massive Particle (WIMP) in direct DM detection [25–41].

In this work we investigate both the tree-level and loop-level contributions to the $\text{CE}\nu\text{NS}$ and the DM DD in the framework of a simplified neutrinophilic DM model. We assume generic DM-neutrino currents interacting with SM quarks through a light spin-0 mediator with general CP phases. For the $\text{CE}\nu\text{NS}$ process, besides the scattering $\nu N \rightarrow \chi N$ with neutrinos converting to DM at tree-level, the loop diagrams can also induce elastic scattering $\nu N \rightarrow \nu N$ with the interme-

diate DM particle χ inside the loops. This additional contribution will affect the fit to COHERENT data and play an important role when the scattering process $\nu N \rightarrow \chi N$ is kinematically forbidden or the scalar current $\bar{q}qa$ is absent. With the incoming DM particle towards the nuclear target, the tree-level and loop-level contributions lead to absorption and scattering detection strategies, respectively. The DM absorption process $\chi N \rightarrow \nu N$ exhibits an enhanced nuclear recoil energy and is sensitive to the lighter DM in the MeV regime. The ordinary elastic scattering off a nucleus $\chi N \rightarrow \chi N$ induced by neutrinos in the loop diagrams can probe GeV scale WIMP DM.

This paper is organized as follows. In Sec. II we describe the simplified neutrinophilic DM model. In Sec. III and IV we present the analytical expressions of the CE ν NS cross section and the cross section of DM scattering off a nucleus, respectively. Both the tree-level and loop-level contributions are given in general forms. The numerical results are also shown. We discuss other relevant constraints on this model in Sec. V. Our conclusions are drawn in Sec. VI. Some calculational details are collected in the Appendix.

II. SIMPLIFIED NEUTRINOPHILIC DARK MATTER MODEL

We consider a Dirac fermion χ charged under lepton number as the DM candidate being a SM gauge singlet. It is generally viewed as the sterile neutrino but can be a generic singlet fermion which mixes with the neutrino fields ν . In the simplified neutrinophilic DM model, the neutrinos interact with DM particle χ through a spin-0 field a and the mediator a couples to the SM quarks as

$$\mathcal{L} \supset g_\chi a \bar{\chi} \left(\cos \theta_\chi + i \gamma_5 \sin \theta_\chi \right) \nu + \sum_q g_q a \bar{q} \left(\cos \theta_q + i \gamma_5 \sin \theta_q \right) q + h.c. , \quad (1)$$

where θ_χ denotes the relative CP phase angle between ν and χ , and θ_q is the CP phase in quark sector. Here we use a universal coupling g_q for the interaction between SM quarks and the mediator a . In practice, below we perform a generic hypothesis with different g_q couplings for up-type and down-type quarks. This hypothesis can be realized in the two-Higgs-doublet model (2HDM) [31, 32, 42] and one will see that the flavor constraints can be relaxed in this choice. The choice of $(\theta_\chi, \theta_q) = (0, 0)$ is exactly the case with pure scalar mediator studied in Ref. [20]. The other CP conserving case is $(\theta_\chi, \theta_q) = (\pi/2, \pi/2)$ with the field a being a pseudoscalar mediator. Generally, the scenario with $\theta_q = \pi/2$ leads to suppressed SD interaction at tree-level and the detectable signals are absent in both neutrino and DM DD experiments.

One should note that the above simplified hypothesis does not respect gauge invariance prior to the SM electroweak symmetry breaking. Thus, we expect that there exist additional couplings between a and the SM Higgs in specific UV complete models [31]. Without loss of generality, we introduce a scalar trilinear coupling

$$\mathcal{L} \supset \frac{1}{2} \lambda_{haa} v_0 h a^2 , \quad (2)$$

where $v_0 = (\sqrt{2}G_F)^{-1/2} \simeq 246$ GeV is the SM Higgs vacuum expectation value (vev). We will show that this interaction induces additional loop diagram in the scattering process.

In Fig. 1 we show the diagrams for the processes of neutrino or DM interacting with the nucleus target at quark-level. For incoming neutrino (DM) processes, $A = \nu(\chi), B = \chi(\nu)$. The tree-level diagram in Fig. 1 (a) is generated by two vertices from the two couplings in the Lagrangian given in Eq. (1) and a mediator a in t channel. Fig. 1 (b) is a triangle diagram intermediated by the λ_{haa} coupling and the SM Higgs field h . Figs. 1 (c) and (d) are the box diagrams formed by two a fields in the internal lines. Recent developments in the loop calculation include the contributions from two-loop scattering diagrams in Figs. 1 (e) and (f) for scalar-type gluon operator $\frac{\alpha_s}{\pi} G_{\mu\nu}^a G^{a\mu\nu}$ [31, 33, 35]. The full two-loop calculation can be obtained by integrating out the heavy quarks and the mediators in the loops. In next sections we will display how the effective operators for the neutrino and DM scattering are formed from these diagrams.

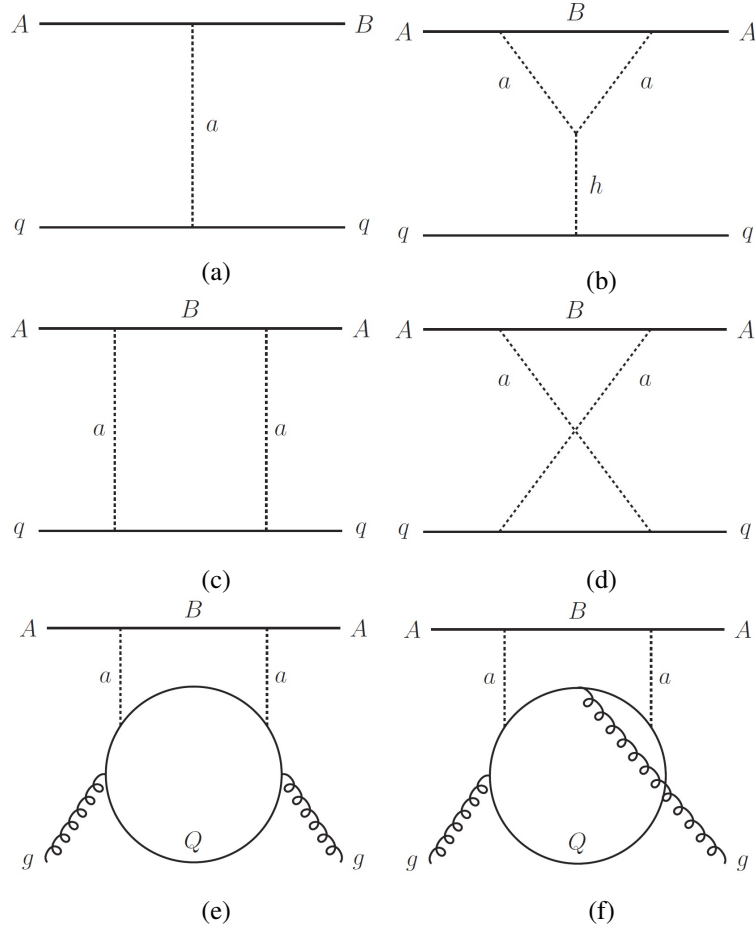


FIG. 1. Diagrams for the processes of neutrino or DM interacting with quark or gluon. For incoming neutrino processes, $A = \nu, B = \chi$. For incoming DM processes, $A = \chi, B = \nu$.

III. COHERENT ELASTIC NEUTRINO-NUCLEUS SCATTERING

For the incoming neutrino scattering $\nu(p_1)q(k_1) \rightarrow \chi(p_2)q(k_2)$ in Fig. 1 (a) with $A = \nu, B = \chi$, we obtain the tree-level matrix element

$$iM_{\text{tree}} = \sum_{q=\text{all}} \frac{-i}{t - m_a^2} g_\chi g_q \bar{\chi}(p_2) (c_{\theta_\chi} + i\gamma_5 s_{\theta_\chi}) P_L \nu(p_1) [c_{\theta_q} \bar{q}(k_2) q(k_1) + s_{\theta_q} \bar{q}(k_2) i\gamma_5 q(k_1)] , \quad (3)$$

where $P_L = \frac{1-\gamma_5}{2}$, the Mandelstam variable $t = (p_1 - p_2)^2$ and $c_x \equiv \cos(x), s_x \equiv \sin(x)$. When $(\theta_\chi, \theta_q) = (0, 0)$, this is exactly the case in Ref. [20] with scalar mediator. In the case of $\theta_q = \pi/2$, the SI contribution from tree-level diagram to the neutrino-nucleus scattering is zero.

For the elastic scattering process $\nu(p_1)q(k_1) \rightarrow \nu(p_2)q(k_2)$, there are multiple loop-level contributions as shown in Fig. 1. We first consider the one-loop triangle diagram with SM Higgs exchange and the matrix element is

$$iM_{\text{triangle}} = \sum_{q=\text{all}} \frac{-i\lambda_{haa} v_0 m_\chi g_\chi^2}{(4\pi)^2 (t - m_h^2)} C_0[p_1^2, (p_1 - p_2)^2, p_2^2; m_\chi^2, m_a^2, m_a^2] \times \bar{\nu}(p_2) (c_{2\theta_\chi} + i\gamma_5 s_{2\theta_\chi}) P_L \nu(p_1) \bar{q}(k_2) q(k_1) . \quad (4)$$

In the zero momentum transfer limit $t \rightarrow 0$ and taking massless neutrinos, the Passarino-Veltman function C_0 can be simplified as shown in the Appendix. One can see that the quark current is pure scalar-type in this diagram due to the SM Higgs exchange. The matrix element of the one-loop box diagrams is

$$\begin{aligned} iM_{\text{box}} = & \sum_{q=u,d,s} \frac{i}{(4\pi)^2} g_\chi^2 g_q^2 \frac{4m_\chi m_q}{m_a^2} D_{00} \bar{\nu}(p_2) (c_{2\theta_\chi} + i\gamma_5 s_{2\theta_\chi}) P_L \nu(p_1) \bar{q}(k_2) q(k_1) \\ & + \sum_{q=u,d,s} \frac{i}{(4\pi)^2} g_\chi^2 g_q^2 4m_\chi m_q c_{\theta_q} D_0 \bar{\nu}(p_2) (c_{2\theta_\chi} + i\gamma_5 s_{2\theta_\chi}) P_L \nu(p_1) \bar{q}(k_2) (c_{\theta_q} + i\gamma_5 s_{\theta_q}) q(k_1) \\ & + \sum_{q=u,d,s,c,b} \frac{i}{(4\pi)^2} g_\chi^2 g_q^2 \frac{8}{m_a^2} D_{001} \bar{\nu}(p_2) i\partial^\mu \gamma^\nu P_L \nu(p_1) O_{\mu\nu}^q \\ & + \sum_{q=u,d,s,c,b} \frac{i}{(4\pi)^2} g_\chi^2 g_q^2 \frac{4m_\chi}{m_a^2} D_{11} \bar{\nu}(p_2) (c_{2\theta_\chi} + i\gamma_5 s_{2\theta_\chi}) i\partial^\mu i\partial^\nu P_L \nu(p_1) O_{\mu\nu}^q , \end{aligned} \quad (5)$$

where $O_{\mu\nu}^q$ is the twist-2 operator for quark

$$O_{\mu\nu}^q = \frac{i}{2} \bar{q} \left(\partial_\mu \gamma_\nu + \partial_\nu \gamma_\mu - \frac{1}{2} g_{\mu\nu} \not{\partial} \right) q . \quad (6)$$

The Passarino-Veltman functions are also collected in the Appendix.

For the heavy quark loops in the two-loop diagrams, we calculate the amplitude using the Fock-Schwinger gauge for the gluon background field [26, 43]. First, the amplitude contributing to the effective operator $aaG_{\mu\nu}^a G^{a\mu\nu}$ is

$$iM_{aaGG} = i\Pi_G(\ell^2) \frac{\alpha_s}{12\pi} G_{\rho\sigma}^a G^{a\rho\sigma} + i\Pi_{\tilde{G}}(\ell^2) \frac{\alpha_s}{8\pi} G_{\rho\sigma}^a \tilde{G}^{a\rho\sigma} , \quad (7)$$

where $G^{a\mu\nu}$ is the gluon field strength tensor and $\tilde{G}^{a\mu\nu} = \frac{1}{2}\epsilon^{\mu\nu\alpha\beta}G_{\alpha\beta}^a$. Then, the complete two-loop matrix element in Figs. 1 (e) and (f) reads

$$\begin{aligned}
iM_{2\text{-loop}} &= -g_\chi^2 \int \frac{d^4\ell}{(2\pi)^4} \bar{\nu}(p_2) [\ell + m_\chi (c_{2\theta_\chi} + i\gamma_5 s_{2\theta_\chi})] P_L \nu(p_1) \\
&\times \frac{1}{[(\ell + p_1)^2 - m_\chi^2](\ell^2 - m_a^2)^2} \left[\Pi_G(\ell^2) \frac{\alpha_s}{12\pi} G_{\rho\sigma}^a G^{a\rho\sigma} + \Pi_{\tilde{G}}(\ell^2) \frac{\alpha_s}{8\pi} G_{\rho\sigma}^a \tilde{G}^{a\rho\sigma} \right] \\
&= \left[C_{G,S} \bar{\nu}(p_2) P_L \nu(p_1) + C_{G,PS} \bar{\nu}(p_2) i\gamma_5 P_L \nu(p_1) \right] \frac{-\alpha_s}{12\pi} G_{\rho\sigma}^a G^{a\rho\sigma} \\
&+ \left[C_{\tilde{G},S} \bar{\nu}(p_2) P_L \nu(p_1) + C_{\tilde{G},PS} \bar{\nu}(p_2) i\gamma_5 P_L \nu(p_1) \right] \frac{\alpha_s}{8\pi} G_{\rho\sigma}^a \tilde{G}^{a\rho\sigma}, \tag{8}
\end{aligned}$$

where ℓ denotes the momentum of the mediator a and

$$C_{G,S} = \frac{i}{(4\pi)^2} \sum_{Q=c,b,t} g_\chi^2 g_Q^2 m_\chi c_{2\theta_\chi} F_G(p_1^2, m_\chi^2, m_a^2, m_Q^2), \tag{9}$$

$$C_{G,PS} = \frac{i}{(4\pi)^2} \sum_{Q=c,b,t} g_\chi^2 g_Q^2 m_\chi s_{2\theta_\chi} F_G(p_1^2, m_\chi^2, m_a^2, m_Q^2), \tag{10}$$

$$C_{\tilde{G},S} = -\frac{i}{(4\pi)^2} \sum_{Q=c,b,t} g_\chi^2 g_Q^2 m_\chi c_{2\theta_\chi} F_{\tilde{G}}(p_1^2, m_\chi^2, m_a^2, m_Q^2), \tag{11}$$

$$C_{\tilde{G},PS} = -\frac{i}{(4\pi)^2} \sum_{Q=c,b,t} g_\chi^2 g_Q^2 m_\chi s_{2\theta_\chi} F_{\tilde{G}}(p_1^2, m_\chi^2, m_a^2, m_Q^2). \tag{12}$$

The above $\Pi_G(\ell^2)$, $\Pi_{\tilde{G}}(\ell^2)$ and $F_G, F_{\tilde{G}}$ functions are all given in the Appendix.

The nucleon form factors are defined as [44, 45]

$$\langle N | m_q \bar{q} q | N \rangle = m_N f_q^N \bar{N} N, \quad q = u, d, s, \tag{13}$$

$$\langle N | m_Q \bar{Q} Q | N \rangle = \langle N | \frac{-\alpha_s}{12\pi} G_{\mu\nu}^a G^{a\mu\nu} | N \rangle = \frac{2}{27} m_N f_G^N \bar{N} N, \quad Q = c, b, t, \tag{14}$$

$$\langle N | O_{\mu\nu}^q | N \rangle = \frac{1}{m_N} \left(p_\mu^N p_\nu^N - \frac{1}{4} m_N^2 g_{\mu\nu} \right) \left(q^N(2) + \bar{q}^N(2) \right) \bar{N} N, \quad q = u, d, s, c, b, \tag{15}$$

for the SI interactions and those for SD interactions are

$$\langle N | m_q \bar{q} i\gamma_5 q | N \rangle = F_P^{q/N}(q^2) \bar{N} i\gamma_5 N, \quad q = u, d, s, \tag{16}$$

$$\langle N | m_Q \bar{Q} i\gamma_5 Q | N \rangle = \langle N | \frac{\alpha_s}{8\pi} G_{\mu\nu}^a \tilde{G}^{a\mu\nu} | N \rangle = F_{\tilde{G}}^N(q^2) \bar{N} i\gamma_5 N, \quad Q = c, b, t. \tag{17}$$

Next, we can obtain the matrix elements at nucleon-level

$$\begin{aligned}
iM_{\text{tree}}^N &= \frac{-i}{t - m_a^2} g_\chi g_q c_{\theta_q} \left(\sum_{q=u,d,s} \frac{m_N}{m_q} f_q^N + \sum_{Q=c,b,t} \frac{2}{27} \frac{m_N}{m_Q} f_G^N \right) \\
&\times \bar{\chi}(p_2) (c_{\theta_\chi} + i\gamma_5 s_{\theta_\chi}) P_L \nu(p_1) \bar{N}(k_2) N(k_1) + \boxed{\text{SD}}, \tag{18}
\end{aligned}$$

$$iM_{\text{triangle}}^N = \frac{-i\lambda_{haa} v_0 m_\chi g_\chi^2}{(4\pi)^2 (t - m_h^2)} C_0 \left(\sum_{q=u,d,s} \frac{m_N}{m_q} f_q^N + \sum_{Q=c,b,t} \frac{2}{27} \frac{m_N}{m_Q} f_G^N \right)$$

$$\times \bar{\nu}(p_2)(c_{2\theta_\chi} + i\gamma_5 s_{2\theta_\chi})P_L\nu(p_1)\bar{N}(k_2)N(k_1), \quad (19)$$

$$iM_{\text{box}}^N = \sum_{q=u,d,s} \frac{i}{(4\pi)^2} g_\chi^2 g_q^2 f_q^N \left(\frac{4m_\chi m_N}{m_a^2} D_{00} + 4m_\chi m_N c_{\theta_q}^2 D_0 \right) \\ \times \bar{\nu}(p_2)(c_{2\theta_\chi} + i\gamma_5 s_{2\theta_\chi})P_L\nu(p_1)\bar{N}(k_2)N(k_1) + \boxed{\text{SD}}, \quad (20)$$

$$iM_{2\text{-loop}}^N = \left[C_{G,S}\bar{\nu}(p_2)P_L\nu(p_1) + C_{G,PS}\bar{\nu}(p_2)i\gamma_5 P_L\nu(p_1) \right] \frac{2}{27} m_N f_G^N \bar{N}(k_2)N(k_1) + \boxed{\text{SD}} \quad (21)$$

Here $\boxed{\text{SD}}$ stands for SD terms which will be omitted in the following calculation.

Since χ is not detected in a neutrino scattering experiment, the total differential cross section of $\text{CE}\nu\text{NS}$ can be written as

$$\frac{d\sigma}{dT} = \frac{d\sigma_{\text{SM}}}{dT} + \frac{d\sigma_{\text{tree}}}{dT} + \frac{d\sigma_{\text{loop}}}{dT}, \quad (22)$$

where T is the nuclear recoil energy. The SM differential cross section is given by

$$\frac{d\sigma_{\text{SM}}}{dT} = \frac{G_F^2 M}{2\pi} [Zg_p^V + Ng_n^V]^2 F^2(Q^2) \left(2 - \frac{MT}{E^2} \right), \quad (23)$$

where $F(Q^2)$ refers to the nuclear form factor with the moment transfer $Q^2 = 2MT$. Here M is the mass of target nucleus, E is the incoming neutrino energy, Z (N) is the number of protons (neutrons) in the target nucleus, $g_n^V = -\frac{1}{2}$ and $g_p^V = \frac{1}{2} - 2\sin^2\theta_W$ are the SM weak couplings with θ_W being the weak mixing angle.

From Eq. (18), the tree-level differential cross section of $\nu N \rightarrow \chi N$ is

$$\frac{d\sigma_{\text{tree}}}{dT} = \frac{g_\chi^2 g_N^2 F^2(Q^2)}{16\pi E^2 (m_a^2 + 2MT)^2} (2M + T) (2MT + m_\chi^2), \quad (24)$$

where

$$g_N = Zm_p \left(\sum_{q=u,d,s} \frac{f_q^p}{m_q} + \sum_{Q=c,b,t} \frac{2}{27} \frac{f_Q^p}{m_Q} \right) g_q c_{\theta_q} + Nm_n \left(\sum_{q=u,d,s} \frac{f_q^n}{m_q} + \sum_{Q=c,b,t} \frac{2}{27} \frac{f_Q^n}{m_Q} \right) g_q c_{\theta_q}. \quad (25)$$

Note that in order to produce a massive DM χ in the scattering $\nu N \rightarrow \chi N$, the energy of the incident neutrinos should be larger than a minimal energy [18, 19], i.e.,

$$E > m_\chi + \frac{m_\chi^2}{2M}. \quad (26)$$

From Eqs. (19), (20) and (21), we can write the loop-level differential cross section as

$$\frac{d\sigma_{\text{loop}}}{dT} = \frac{G_{\text{loop}}^2 M}{8\pi E^2} F^2(Q^2) (2MT + T^2), \quad (27)$$

where

$$\begin{aligned}
G_{\text{loop}} = & \frac{Z}{(4\pi)^2} g_\chi^2 m_\chi m_p \left[\frac{\lambda_{haa} v_0}{2MT + m_h^2} \left(\sum_{q=u,d,s} \frac{f_q^p}{m_q} + \sum_{Q=c,b,t} \frac{2}{27} \frac{f_G^p}{m_Q} \right) C_0 \right. \\
& + 4 \sum_{q=u,d,s} g_q^2 f_q^p \left(\frac{D_{00}}{m_a^2} + c_{\theta_q}^2 D_0 \right) + \frac{2}{27} f_G^p \sum_{Q=c,b,t} g_Q^2 F_G(p_1^2, m_\chi^2, m_a^2, m_Q^2) \left. \right] \\
& + \frac{N}{(4\pi)^2} g_\chi^2 m_\chi m_n \left[\frac{\lambda_{haa} v_0}{2MT + m_h^2} \left(\sum_{q=u,d,s} \frac{f_q^n}{m_q} + \sum_{Q=c,b,t} \frac{2}{27} \frac{f_G^n}{m_Q} \right) C_0 \right. \\
& + 4 \sum_{q=u,d,s} g_q^2 f_q^n \left(\frac{D_{00}}{m_a^2} + c_{\theta_q}^2 D_0 \right) + \frac{2}{27} f_G^n \sum_{Q=c,b,t} g_Q^2 F_G(p_1^2, m_\chi^2, m_a^2, m_Q^2) \left. \right]. \tag{28}
\end{aligned}$$

One can see that the total differential cross section has no dependence on the mixing angle θ_χ . This is because the tree-level amplitude and the loop-level amplitude have no interference in this case and the neutrinos in the external legs are nearly massless. The measurement of the SM Higgs decay at the LHC [46] implies the constraint on the coupling $\lambda_{haa} \lesssim 0.01$ [35]. The flavor physics also sets stringent constraints on the coupling g_q for up-type quarks as discussed below. Thus, in the numerical calculation, we neglect the coupling for up-type quarks and the triangle diagram and the two-loop diagrams dominated by top quark contribution. We checked that this ignorance does not affect our conclusion. For the nucleon form factors in SI interactions, we adopt the default values in micrOMEGAs [47, 48].

The CE ν NS process has been recently observed by the COHERENT experiment in a low-threshold CsI detector at the 6.7σ CL. The neutrinos measured at COHERENT are generated from the Spallation Neutron Source (SNS), and their fluxes are well known and given by

$$\begin{aligned}
\phi_{\nu_\mu}(E_{\nu_\mu}) &= \mathcal{N}_0 \frac{2m_\pi}{m_\pi^2 - m_\mu^2} \delta \left(1 - \frac{2E_{\nu_\mu} m_\pi}{m_\pi^2 - m_\mu^2} \right), \\
\phi_{\nu_e}(E_{\nu_e}) &= \mathcal{N}_0 \frac{192}{m_\mu} \left(\frac{E_{\nu_e}}{m_\mu} \right)^2 \left(\frac{1}{2} - \frac{E_{\nu_e}}{m_\mu} \right), \\
\phi_{\bar{\nu}_\mu}(E_{\bar{\nu}_\mu}) &= \mathcal{N}_0 \frac{64}{m_\mu} \left(\frac{E_{\bar{\nu}_\mu}}{m_\mu} \right)^2 \left(\frac{3}{4} - \frac{E_{\bar{\nu}_\mu}}{m_\mu} \right), \tag{29}
\end{aligned}$$

where \mathcal{N}_0 is a normalization factor determined by the setup of the COHERENT experiment. The ν_μ component is produced from the stopped pion decays, $\pi^+ \rightarrow \mu^+ + \nu_\mu$, which yield a monoenergetic flux at $(m_\pi^2 - m_\mu^2)/(2m_\pi) \simeq 30$ MeV. The $\bar{\nu}_\mu$ and ν_e components are produced from the subsequent muon decays, $\mu^+ \rightarrow e^+ + \bar{\nu}_\mu + \nu_e$, and their energies have a kinematic upper bound at $m_\mu/2 \simeq 53$ MeV.

The presence of DM-neutrino interaction will modify the COHERENT spectrum, which can be seen in Fig. 2. We select two benchmark points to illustrate the effects of modified spectra:

- Case A: $\theta_q = 0$, $m_\chi = 10$ MeV, $m_a = 100$ MeV, and $g_\chi g_q = 5.0 \times 10^{-9}$,

- Case B: $\theta_q = \pi/2$, $m_\chi = 100$ MeV, $m_a = 200$ MeV, and $g_\chi g_q = 0.01$.

In Case A, the modification to the SM spectrum is dominated by the tree-level scattering process, $\nu N \rightarrow \chi N$, and the loop-level contribution is negligible due to the small coupling constants. In Case B, since $m_\chi \gtrsim 53$ MeV, the tree-level process is kinematically forbidden, and the modification to the SM spectrum is only contributed by the loop-level diagrams.

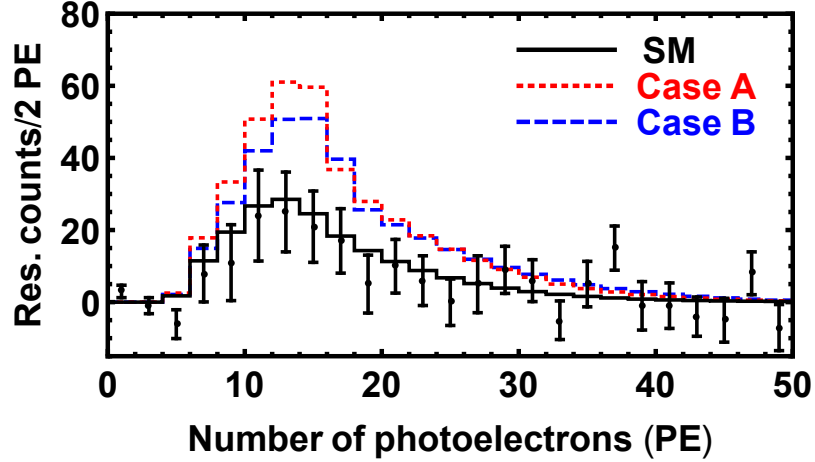


FIG. 2. The expected CE ν NS residual event as a function of the number of photoelectrons at COHERENT. The black solid lines correspond to the SM case, and the red dotted (blue dashed) lines correspond to Case A (B) with $\theta_q = 0$, $m_\chi = 10$ MeV, $m_a = 100$ MeV, and $g_\chi g_q = 5.0 \times 10^{-9}$ ($\theta_q = \pi/2$, $m_\chi = 100$ MeV, $m_a = 200$ MeV, and $g_\chi g_q = 0.01$).

Following Ref. [19], we evaluate the statistical significance of BSM by defining

$$\chi^2 = \sum_{i=4}^{15} \left[\frac{N_{\text{meas}}^i - N_{\text{th}}^i(1 + \alpha) - B_{\text{on}}(1 + \beta)}{\sigma_{\text{stat}}^i} \right]^2 + \left(\frac{\alpha}{\sigma_\alpha} \right)^2 + \left(\frac{\beta}{\sigma_\beta} \right)^2, \quad (30)$$

where N_{meas}^i and N_{th}^i denotes the number of measured (predicted) events per energy bin, respectively. α (β) represents the nuisance parameters for the signal rate (the beam-on background) with a uncertainty of $\sigma_\alpha = 0.28$ ($\sigma_\beta = 0.25$) [24]. The statistical uncertainty per energy bin is calculated by $\sigma_{\text{stat}}^i = \sqrt{N_{\text{meas}}^i + 2B_{\text{SS}}^i + B_{\text{on}}^i}$ with B_{SS} being the steady-state background from the anti-coincident data, and B_{on} the beam-on background mainly consists of prompt neutrons.

To obtain the bounds on the neutrinophilic DM model, we first set $\theta_q = 0$ and $m_a = 2m_\chi$ or $10m_\chi$, and scan over possible values of the product of the coefficients $g_\chi g_q$ for a given m_χ . The 90% CL upper bounds on $g_\chi g_q$ as a function of m_χ are shown in Fig. 3. As we see from Fig. 3, for $m_\chi \lesssim 53$ MeV, the upper bounds on $g_\chi g_q$ are very strong, and can reach as small as 10^{-9} for $m_\chi = 1$ MeV. For $m_\chi \gtrsim 53$ MeV, however, the tree-level process $\nu N \rightarrow \chi N$ is kinematically forbidden and the bounds become much weaker since the contribution from the loop diagrams is relatively small. Thus, there exhibits a kink around $m_\chi \simeq 53$ MeV. Compare the left panel of

Fig. 3 to the right panel, we see that in general the bounds become weaker as the mediator mass increases.

We also fix $\theta_q = \pi/2$ and obtain the 90% CL upper bounds on $g_\chi g_q$ as a function of m_χ . The results are shown in the left and right panel of Fig. 4 for $m_a = 2m_\chi$ and $m_a = 10m_\chi$, respectively. From Eq. (25), we see that for $\theta_q = \pi/2$, the SI terms from the tree-level process vanish, and the bounds are mainly determined by the loop-level contribution¹. For $m_\chi \simeq 53$ MeV, the pure loop-level contribution constrains $g_\chi g_q$ to be smaller than 0.003 (0.06) for $m_a = 2m_\chi$ ($10m_\chi$).

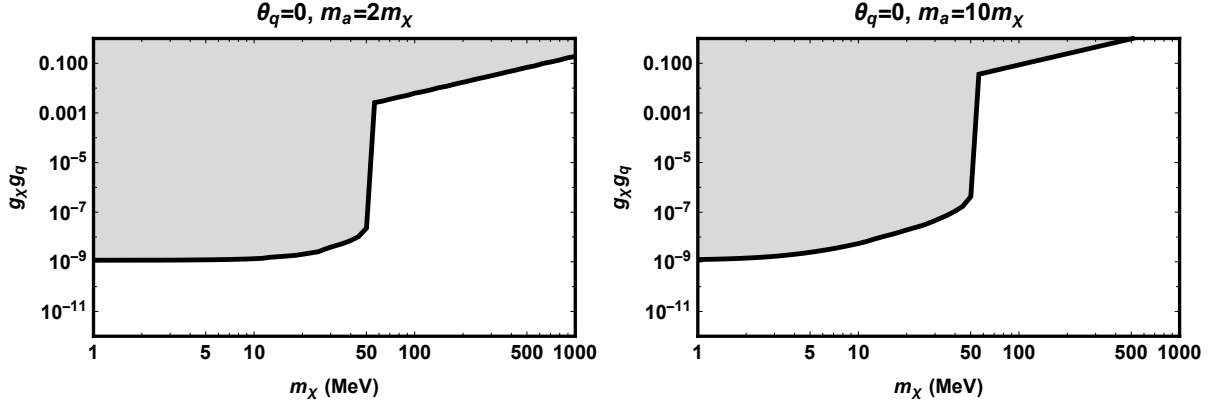


FIG. 3. The 90% CL upper bounds on $g_\chi g_q$ as a function of the DM mass m_χ from COHERENT. We assume $\theta_q = 0$ and $m_a = 2m_\chi$ (left), or $m_a = 10m_\chi$ (right).

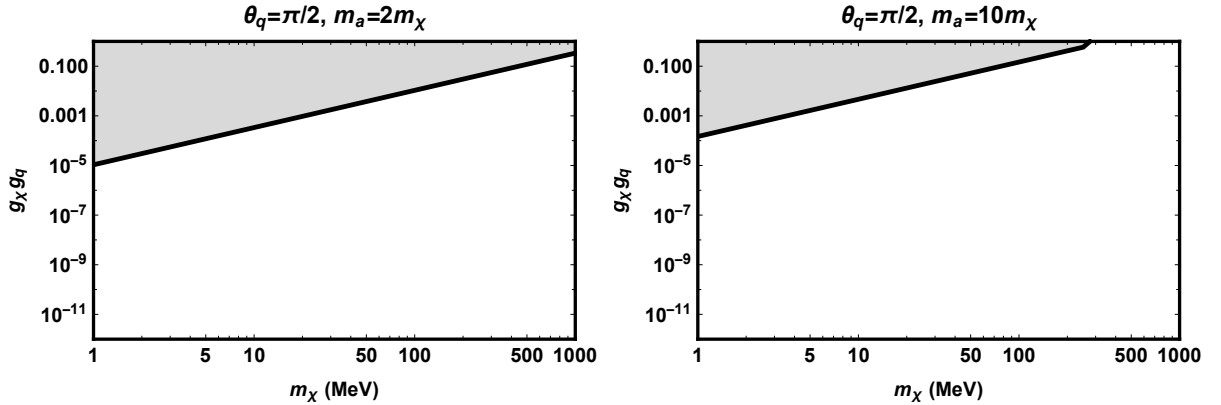


FIG. 4. Same as Fig. 3, except for $\theta_q = \pi/2$.

¹ In principle, for $m_\chi \lesssim 53$ MeV, the SD terms also contribute to the CE ν NS process. The contribution is nonzero for the odd-even nucleus in the CsI detector. As it is highly suppressed compared with the SI terms, we do not consider its contribution here.

IV. DIRECT DM DETECTION

At tree-level, the DM absorption is the reversed process with respect to that for the above neutrino scattering. For $\chi(p_1)q(k_1) \rightarrow \nu(p_2)q(k_2)$, we obtain the tree-level matrix element

$$iM_{\text{tree}} = \sum_{q=\text{all}} \frac{-i}{t - m_a^2} g_\chi g_q \bar{\nu}(p_2) (c_{\theta_\chi} + i\gamma_5 s_{\theta_\chi}) \chi(p_1) [c_{\theta_q} \bar{q}(k_2) q(k_1) + s_{\theta_q} \bar{q}(k_2) i\gamma_5 q(k_1)] , \quad (31)$$

with the Mandelstam variable $t = (p_1 - p_2)^2$. Again, in the case of $\theta_q = \pi/2$, the SI contribution from tree-level diagram to the DM absorption is zero. For the elastic scattering with incoming χ , i.e. $\chi(p_1)q(k_1) \rightarrow \chi(p_2)q(k_2)$, the neutrinos are in the internal lines. Again we first consider the one-loop diagram with SM Higgs exchange and the matrix element is

$$iM_{\text{triangle}} = N_\nu \sum_{q=\text{all}} \frac{i\lambda_{haa} v_0 m_\chi g_\chi^2}{(4\pi)^2 (t - m_h^2)} (C_1 + C_2) \bar{\chi}(p_2) \chi(p_1) \bar{q}(k_2) q(k_1) , \quad (32)$$

where $N_\nu = 3$ is the number of active neutrinos. We also collect the Passarino-Veltman functions here and below in the Appendix. The matrix element of the one-loop box diagram is

$$\begin{aligned} iM_{\text{box}} = & N_\nu \sum_{q=u,d,s} \frac{i}{(4\pi)^2} g_\chi^2 g_q^2 \frac{4}{m_a^2} \left[\frac{3}{2} m_\chi m_q D_{001} \bar{\chi}(p_2) \chi(p_1) \bar{q}(k_2) q(k_1) \right. \\ & + \left. \frac{1}{4} m_\chi^3 m_q D_{111} \bar{\chi}(p_2) \chi(p_1) \bar{q}(k_2) q(k_1) \right] \\ & + N_\nu \sum_{q=u,d,s} \frac{i}{(4\pi)^2} g_\chi^2 g_q^2 \frac{4m_\chi}{m_a^2} \left[m_q D_{00} \bar{\chi}(p_2) \chi(p_1) \bar{q}(k_2) q(k_1) \right. \\ & + \left. \frac{1}{4} m_\chi^2 m_q D_{11} \bar{\chi}(p_2) \chi(p_1) \bar{q}(k_2) q(k_1) \right] \\ & + N_\nu \sum_{q=u,d,s} \frac{i}{(4\pi)^2} g_\chi^2 g_q^2 4m_\chi m_q c_{\theta_q} (D_0 + D_1) \bar{\chi}(p_2) \chi(p_1) \bar{q}(k_2) (c_{\theta_q} + i\gamma_5 s_{\theta_q}) q(k_1) \\ & + N_\nu \sum_{q=u,d,s,c,b} \frac{i}{(4\pi)^2} g_\chi^2 g_q^2 \frac{4}{m_a^2} \left[2D_{001} \bar{\chi}(p_2) i\partial^\mu \gamma^\nu \chi(p_1) O_{\mu\nu}^q + m_\chi D_{111} \bar{\chi}(p_2) i\partial^\mu i\partial^\nu \chi(p_1) O_{\mu\nu}^q \right] \\ & + N_\nu \sum_{q=u,d,s,c,b} \frac{i}{(4\pi)^2} g_\chi^2 g_q^2 \frac{4m_\chi}{m_a^2} \left[D_{11} \bar{\chi}(p_2) i\partial^\mu i\partial^\nu \chi(p_1) O_{\mu\nu}^q \right] . \end{aligned} \quad (33)$$

Following the same procedure mentioned above, the two-loop matrix element is

$$\begin{aligned} iM_{2\text{-loop}} = & -N_\nu g_\chi^2 \int \frac{d^4\ell}{(2\pi)^4} \bar{\chi}(p_2) (\ell + m_\chi) \chi(p_1) \\ & \times \frac{1}{(\ell + p_1)^2 (\ell^2 - m_a^2)^2} \left[\Pi_G(\ell^2) \frac{\alpha_s}{12\pi} G_{\rho\sigma}^a G^{a\rho\sigma} + \Pi_{\tilde{G}}(\ell^2) \frac{\alpha_s}{8\pi} G_{\rho\sigma}^a \tilde{G}^{a\rho\sigma} \right] \\ & = N_\nu \left[C_{G,S} \bar{\chi}(p_2) \chi(p_1) \frac{-\alpha_s}{12\pi} G_{\rho\sigma}^a G^{a\rho\sigma} + C_{\tilde{G},S} \bar{\chi}(p_2) \chi(p_1) \frac{\alpha_s}{8\pi} G_{\rho\sigma}^a \tilde{G}^{a\rho\sigma} \right] , \end{aligned} \quad (34)$$

where

$$C_{G,S} = \frac{i}{(4\pi)^2} \sum_{Q=c,b,t} g_\chi^2 g_Q^2 \left[m_\chi F_G(p_1^2, 0, m_a^2, m_Q^2) + m_\chi F'_G(p_1^2, 0, m_a^2, m_Q^2) \right] , \quad (35)$$

$$C_{\bar{G},S} = -\frac{i}{(4\pi)^2} \sum_{Q=c,b,t} g_\chi^2 g_Q^2 \left[m_\chi F_{\bar{G}}(p_1^2, 0, m_a^2, m_Q^2) + m_\chi F'_{\bar{G}}(p_1^2, 0, m_a^2, m_Q^2) \right]. \quad (36)$$

After omitting the SD terms, the matrix elements at nucleon-level are

$$iM_{\text{tree}}^N = \frac{-i}{t - m_a^2} g_\chi g_q c_{\theta_q} \left(\sum_{q=u,d,s} \frac{m_N}{m_q} f_q^N + \sum_{Q=c,b,t} \frac{2}{27} \frac{m_N}{m_Q} f_Q^N \right) \times \bar{\nu}(p_2) (c_{\theta_\chi} + i\gamma_5 s_{\theta_\chi}) \chi(p_1) \bar{N}(k_2) N(k_1) + \boxed{\text{SD}}, \quad (37)$$

$$iM_{\text{triangle}}^N = N_\nu \frac{i\lambda_{haa} v_0 m_\chi g_\chi^2}{(4\pi)^2 (t - m_h^2)} (C_1 + C_2) \left(\sum_{q=u,d,s} \frac{m_N}{m_q} f_q^N + \sum_{Q=c,b,t} \frac{2}{27} \frac{m_N}{m_Q} f_Q^N \right) \times \bar{\chi}(p_2) \chi(p_1) \bar{N}(k_2) N(k_1), \quad (38)$$

$$\begin{aligned} iM_{\text{box}}^N &= N_\nu \sum_{q=u,d,s} \frac{i}{(4\pi)^2} g_\chi^2 g_q^2 f_q^N \frac{4}{m_a^2} \left[\frac{3}{2} m_\chi m_N D_{001} + \frac{1}{4} m_\chi^3 m_N D_{111} \right] \bar{\chi}(p_2) \chi(p_1) \bar{N}(k_2) N(k_1) \\ &+ N_\nu \sum_{q=u,d,s} \frac{i}{(4\pi)^2} g_\chi^2 g_q^2 f_q^N \frac{4m_\chi}{m_a^2} \left[m_N D_{00} + \frac{1}{4} m_\chi^2 m_N D_{11} \right] \bar{\chi}(p_2) \chi(p_1) \bar{N}(k_2) N(k_1) \\ &+ N_\nu \sum_{q=u,d,s} \frac{i}{(4\pi)^2} g_\chi^2 g_q^2 f_q^N 4m_\chi m_N c_{\theta_q}^2 (D_0 + D_1) \bar{\chi}(p_2) \chi(p_1) \bar{N}(k_2) N(k_1) \\ &+ N_\nu \sum_{q=u,d,s,c,b} \frac{i}{(4\pi)^2} g_\chi^2 g_q^2 \left(q^N(2) + \bar{q}^N(2) \right) \\ &\times \frac{4}{m_a^2} \left[2D_{001} \frac{3}{4} m_N m_\chi + m_\chi D_{111} \frac{3}{4} m_N m_\chi^2 \right] \bar{\chi}(p_2) \chi(p_1) \bar{N}(k_2) N(k_1) \\ &+ N_\nu \sum_{q=u,d,s,c,b} \frac{i}{(4\pi)^2} g_\chi^2 g_q^2 \left(q^N(2) + \bar{q}^N(2) \right) \frac{4m_\chi}{m_a^2} D_{11} \frac{3}{4} m_N m_\chi^2 \bar{\chi}(p_2) \chi(p_1) \bar{N}(k_2) N(k_1) \\ &+ \boxed{\text{SD}}, \end{aligned} \quad (39)$$

$$iM_{2\text{-loop}}^N = N_\nu C_{G,S} \frac{2}{27} m_N f_G^N \bar{\chi}(p_2) \chi(p_1) \bar{N}(k_2) N(k_1) + \boxed{\text{SD}}. \quad (40)$$

For the DM absorption from the tree-level diagram, the differential cross section and the differential rate per nuclear recoil energy are [21, 22]

$$\frac{d\sigma_{\text{tree}}}{dE_R} = \frac{|\overline{\mathcal{M}}_T|^2}{16\pi v M_T^2} \delta(E_R - E_R^0), \quad (41)$$

$$\frac{dR}{dE_R} = N_T \frac{\rho_\chi}{m_\chi} \sigma_{\text{NC}} A^2 F^2(q) \delta(E_R - E_R^0) \Theta(E_R^0 - E_{\text{th}}), \quad (42)$$

where N_T is the number of nuclear targets, the local DM density is $\rho_\chi \simeq 0.4 \text{ GeV}/\text{cm}^3$, A is the atomic mass number of the nucleus, Θ is the Heaviside theta function, E_{th} is the experimental threshold, $E_R^0 = m_\chi^2/(2M_T)$ and $\sigma_{\text{NC}} = \frac{m_\chi^2}{4\pi m_a^4} \left[g_\chi g_q c_{\theta_q} \left(\sum_{q=u,d,s} \frac{m_N}{m_q} f_q^N + \sum_{Q=c,b,t} \frac{2}{27} \frac{m_N}{m_Q} f_Q^N \right) \right]^2$.

Here and below we use N and T for nucleon and nuclear quantities, respectively. For the elastic scattering from loop diagrams, we have [49]

$$\frac{d\sigma_{\text{SI}}^T}{dE_R} = \frac{\sigma_{\text{SI}}^N M_T}{2\mu_{\chi N}^2 v^2} \Theta(E_R^0 - E_R), \quad (43)$$

$$\frac{dR}{dE_R} = N_T \frac{\rho_\chi}{m_\chi} \frac{\sigma_{\text{SI}}^N M_T}{2\mu_{\chi T}^2} A^2 F^2(q) g(v_{\text{min}}), \quad (44)$$

$$g(v_{\text{min}}) = \int d^3\vec{v} \frac{f(\vec{v})}{v} \Theta\left(v - \sqrt{\frac{M_T E_R}{2\mu_{\chi T}^2}}\right), \quad (45)$$

with $\mu_{\chi T} = m_\chi M_T / (m_\chi + M_T)$ being the reduced mass for the DM-nucleus system, $E_R^0 = 2\mu_{\chi T}^2 v^2 / M_T$ and $f(\vec{v})$ is the DM velocity distribution. The DM-nucleon SI scattering cross section is given by

$$\sigma_{\text{SI}}^N = \frac{1}{\pi} \left(\frac{m_\chi m_N}{m_\chi + m_N} \right)^2 |C_N|^2, \quad (46)$$

where C_N is the summation of the coefficients in front of $\bar{\chi}(p_2)\chi(p_1)\bar{N}(k_2)N(k_1)$ in the above matrix elements.

In the DM absorption, as seen from Eq. (42), the DM particle deposits its mass energy and the event rate exhibits a sharp peak at $E_R \simeq m_\chi^2 / (2M_T)$. This feature allows the search for lighter DM at MeV regime based on both DD experiments and neutrino experiments with higher energy threshold. In contrast, the nuclear recoil energy for the elastic scattering is decreased by the DM velocity square and is too small to detect the loop diagram effect for sub-GeV DM mass. Refs. [21, 22] presented the projected upper bounds on σ_{NC} at various DD experiments and neutrino experiment by assuming the observation of 10 events. We translate the result to the upper bounds on the coupling product $g_\chi g_q$ as shown in Fig. 5, given $\theta_q = 0$ and $m_a = 2m_\chi$ or $m_a = 10m_\chi$. One can see that the Xenon1T experiment [50] and the solar neutrino experiment Borexino [51] can probe $g_\chi g_q$ as small as 10^{-12} (10^{-11}) for $m_\chi \gtrsim 30$ MeV and $m_a = 2m_\chi$ ($m_a = 10m_\chi$). The CRESST experiment [52] can reach the DM mass less than 2 MeV.

To estimate the sensitivity of elastic DM scattering to the loop diagram, we take $\theta_q = \pi/2$ for illustration. There is no SI DM absorption from the tree-level contribution in this case. In this scenario the DM particle deposits its kinetic energy onto the nucleus target in the detector. The rate distribution spreads over the recoil energy and the scattering is sensitive to the WIMP search in the GeV mass scale. Fig. 6 displays the bound on $g_\chi g_q$ as a function of DM mass m_χ from elastic DM scattering via the loop diagrams. Note that we again neglect the up-type quark coupling and the contributions from triangle diagram and the two-loop diagrams. The light blue region indicates the parameter space excluded by the Xenon1T limit [50] and the light red region can be probed by future experiments above the neutrino floor. For $m_a = 2m_\chi$ ($10m_\chi$), the future DD experiment can probe the coupling product $g_\chi g_q$ as small as 0.02 (0.4). Again, the constraint becomes weaker as the mediator mass increases. The most sensitive DM mass is about 10 GeV.

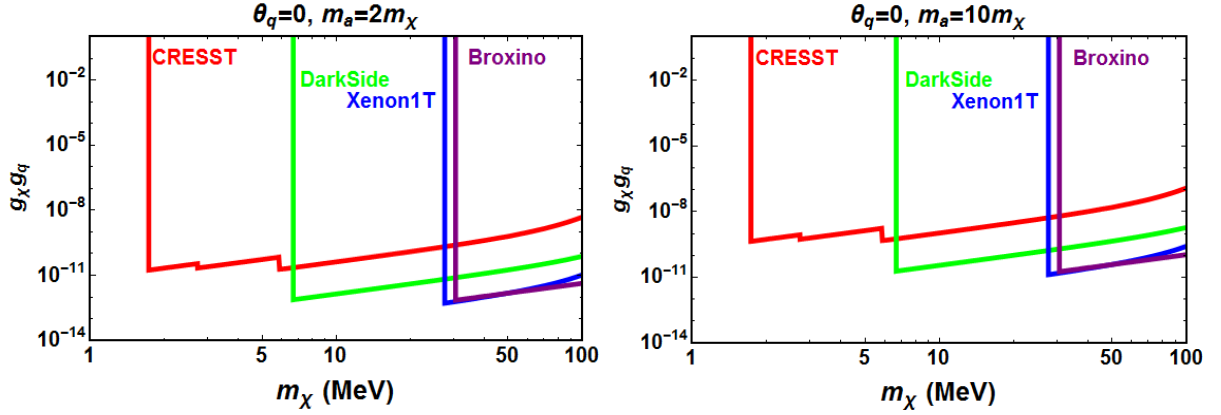


FIG. 5. The upper bounds on $g_\chi g_q$ as a function of DM mass m_χ from DM absorption. We assume $\theta_q = 0$ and $m_a = 2m_\chi$ (left) or $m_a = 10m_\chi$ (right).

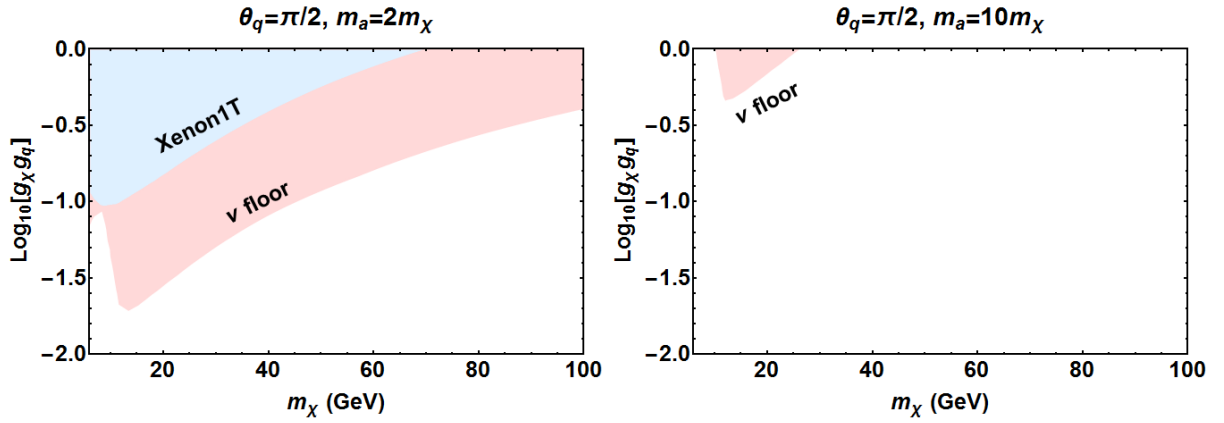


FIG. 6. The bounds on $g_\chi g_q$ as a function of DM mass m_χ from Xenon1T via elastic DM scattering. The Xenon1T experiment [50] excludes the parameter space in the light blue region and the future DD experiments can probe the light red region. The blank region is below the neutrino floor. We assume $\theta_q = \pi/2$ and $m_a = 2m_\chi$ (left) or $m_a = 10m_\chi$ (right).

V. OTHER CONSTRAINTS

A. Stability of decaying DM

In this model the DM particle χ can decay into neutrinos and a photon via a one-loop diagram. Requiring the DM being stable at the Universe time scale would set a very stringent bound on the coupling $g_\chi g_q$ [20]. In spite of this, as argued in Ref. [20], low DM mass can weaken the bound due to the strong DM mass dependence in the decay rate. Also, the additional new physics at high energy scale can cancel the above DM decay at low energy [21].

B. Flavor constraint

The neutrinophilic DM model receives constraints from the invisible rare decays such as $K^+ \rightarrow \pi^+ + \text{invisible}$ via flavor changing neutral currents [53]. This rare decay is recently measured by the NA62 experiment at CERN [54]. In this model the partial width for $K^+ \rightarrow \pi^+ a$ is [55, 56]

$$\Gamma(K^+ \rightarrow \pi^+ a) = \frac{|f(g_q)|^2 + |k(g_q)|^2}{16\pi m_{K^+}^3} \lambda^{1/2}(m_{K^+}^2, m_{\pi^+}^2, m_a^2), \quad (47)$$

$$f(g_q) = \frac{3m_{K^+}^2}{32\pi^2 v_0^2 m_s} g_q \cos \theta_q f_+(0) \sum_{q=u,c,t} m_q^2 V_{qd}^* V_{qs}, \quad (48)$$

$$k(g_q) = \frac{4m_{K^+}^2}{32\pi^2 v_0^2 m_s} g_q \sin \theta_q f_+(0) \sum_{q=u,c,t} m_q^2 V_{qd}^* V_{qs} \ln\left(\frac{m_W^2}{m_q^2}\right), \quad (49)$$

where $\lambda(x, y, z) = x^2 + y^2 + z^2 - 2xy - 2yz - 2xz$ and $f_+(0) \approx 0.9709$ is the vector form factor at zero momentum transfer. For $K_L \rightarrow \pi^0$ decay, one needs to replace $V_{qd}^* V_{qs}$ by $\text{Re}[V_{qd}^* V_{qs}]$ and change the masses of kaon and pion. One can see that the contribution is from the up-type quarks in the loop and Ref. [20] estimated the bound as $g_q \lesssim 1.58 \times 10^{-4}$.

The flavor observables through $K \rightarrow \pi$ transitions thus set stringent constraints on g_q coupling for up-type quarks. We assumed non-universal g_q couplings for up-type and down-type quarks and neglected the up-type quark coupling in the above calculations.

C. DM relic abundance

The thermally averaged cross section of DM pair $\chi\bar{\chi}$ annihilation into a neutrino pair or a pair of a is, to the leading order in DM velocity v ,

$$\langle\sigma v\rangle = \frac{N_\nu g_\chi^4 m_\chi^2}{8\pi(m_\chi^2 + m_a^2)^2} + \frac{N_\nu^2 g_\chi^4}{192\pi m_\chi \sqrt{m_\chi^2 - m_a^2}} v^2 \Theta(m_\chi - m_a). \quad (50)$$

The thermal DM relic abundance is determined by the equation

$$\Omega_\chi h^2 = \frac{1.07 \times 10^9 \text{ GeV}^{-1}}{M_{\text{Pl}}} \frac{x_F}{\sqrt{g_*}} \frac{1}{a + 3b/x_F + 20c/x_F^2}, \quad (51)$$

for the expansion of annihilation cross section $\langle\sigma v\rangle \sim a + bv^2 + cv^4$. Here, $M_{\text{Pl}} \approx 1.22 \times 10^{19}$ GeV is the Planck mass, h is the Hubble parameter, g_* is the number of relativistic degrees of freedom, and T_F is the freeze-out temperature appearing in $x_F = m_\chi/T_F$. We vary x_F and g_* in the range of $20 < x_F < 30$ and $80 < g_* < 100$, respectively, and adopt the relic abundance measured by Planck, i.e. $\Omega_\chi h^2 = 0.1199 \pm 0.0027$. In Fig. 7, we show the lower bound on g_χ as a function of DM mass m_χ by requiring the neutrinophilic DM to occupy a fraction of the observed relic abundance.

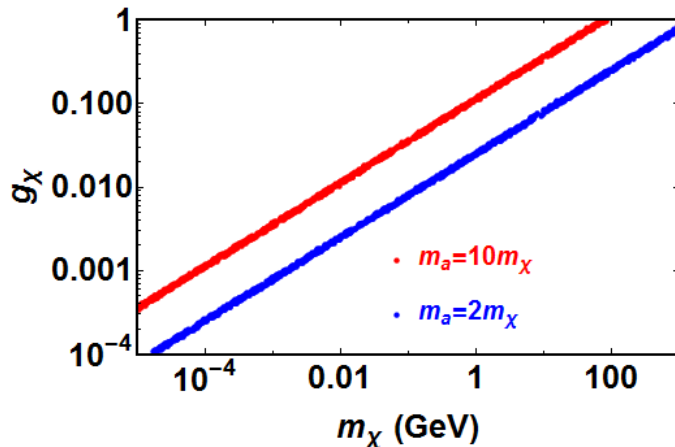


FIG. 7. The lower bound on g_χ as a function of DM mass m_χ from thermal relic abundance. We assume $m_a = 10m_\chi$ or $m_a = 2m_\chi$.

D. LHC constraint

The search for events with large missing transverse momentum with an energetic jet or the third generation SM quarks at the Large Hadron Collider (LHC) may place bounds on the coupling $g_\chi g_q$. One can see that there is no severe bound on the very light DM of interest with spin-0 mediator from monojet search [57, 58] or the coupling of down-type quarks from the production in association with bottom quarks [59]. The most stringent limits are from the associated production of $t\bar{t}$ with missing transverse momentum. The pseudoscalar mediator mass around 20 GeV is excluded at 95% confidence level, assuming the DM mass being 1 GeV and unitary top couplings [60]. This constraint is not severe in our discussion with absent up-type quark coupling. In addition, as stated before, the search for Higgs invisible decay sets constraint on the coupling $\lambda_{h\bar{a}a} \lesssim 0.01$ in a specific Higgs portal model [46, 61].

VI. CONCLUSIONS

We investigate the detection of neutrinophilic DM in both the neutrino and DM experiments. We consider both the tree-level and loop-level contributions to the $CE\nu NS$ and the direct DM detection in the framework of a simplified neutrinophilic DM model with a Dirac fermionic DM χ and a spin-0 mediator a . The couplings between the mediator and the DM χ (the SM quarks) is parameterized by g_χ (g_q). For the CP phase in the quark sector $\theta_q = 0$ ($\pi/2$), the detection processes are dominated by the tree-level (loop-level) contribution. We summarize our main conclusions in the following:

- For $\theta_q = 0$, the COHERENT experiment can set the upper bound of $g_\chi g_q$ as small as 10^{-9}

for $m_\chi = 1$ MeV. Also, by including the loop-level contribution, the COHERENT data is also sensitive to the mass region with $m_\chi \gtrsim 53$ MeV, which is the maximal energy of the incoming neutrinos measured at COHERENT. In general, the bounds become weaker as the mediator mass increases.

- When $\theta_q = \pi/2$, by fitting to the COHERENT data, the loop-level contribution constrains $g_\chi g_q$ as small as 0.003 (0.06) for $m_\chi \simeq 53$ MeV and $m_a = 2m_\chi$ ($10m_\chi$).
- Given $\theta_q = 0$ and incoming DM particle, one can make use of the DM absorption scenario to probe the sub-GeV DM in both DM and neutrino detectors. The Xenon1T experiment and the Borexino experiment can reach $g_\chi g_q$ as small as 10^{-12} (10^{-11}) for $m_\chi \gtrsim 30$ MeV and $m_a = 2m_\chi$ ($m_a = 10m_\chi$). The CRESST experiment is sensitive to the DM as light as $m_\chi \simeq 2$ MeV.
- For $\theta_q = \pi/2$, the elastic DM scattering is induced by the loop diagrams and is sensitive to $m_\chi \simeq 10$ GeV. Future DD DM experiment can probe $g_\chi g_q$ as small as 0.02 (0.4) in this mass regime for $m_a = 2m_\chi$ ($10m_\chi$).

ACKNOWLEDGMENTS

TL is supported by the National Natural Science Foundation of China (Grant No. 11975129) and “the Fundamental Research Funds for the Central Universities”, Nankai University (Grant No. 63196013). JL is supported by the National Natural Science Foundation of China (Grant No. 11905299), Guangdong Basic and Applied Basic Research Foundation (Grant No. 2020A1515011479), the Fundamental Research Funds for the Central Universities, and the Sun Yat-Sen University Science Foundation.

Appendix A: Loop diagram calculation

1. The Passarino-Veltman functions for neutrino-nucleus scattering

For the elastic scattering process $\nu(p_1)q(k_1) \rightarrow \nu(p_2)q(k_2)$, the Passarino-Veltman function for the triangle diagram is

$$C_0[p_1^2, (p_1 - p_2)^2, p_2^2; m_\chi^2, m_a^2, m_a^2] = C_0[0, 0, 0; m_\chi^2, m_a^2, m_a^2] = \frac{m_\chi^2 \ln\left(\frac{m_a^2}{m_\chi^2}\right) - m_a^2 + m_\chi^2}{(m_a^2 - m_\chi^2)^2} \quad (\text{A1})$$

The Passarino-Veltman functions for the one-loop box diagrams are defined as

$$D_0(p_1, m_\chi, m_a) \equiv D_0[p_1^2, p_1^2, 0, 0, 0, p_1^2; 0, m_\chi^2, m_a^2, m_a^2] = \frac{-m_a^2 + m_\chi^2 + m_a^2 \ln\left(\frac{m_a^2}{m_\chi^2}\right)}{m_a^2(m_a^2 - m_\chi^2)^2}, \quad (\text{A2})$$

$$D_{00}(p_1, m_\chi, m_a) \equiv D_{00}[p_1^2, p_1^2, 0, 0, 0, p_1^2; 0, m_\chi^2, 0, m_a^2] - D_{00}[p_1^2, p_1^2, 0, 0, 0, p_1^2; 0, m_\chi^2, m_a^2, m_a^2]$$

$$= \frac{m_a^2 - m_\chi^2 - m_a^2 \ln\left(\frac{m_a^2}{m_\chi^2}\right)}{4(m_a^2 - m_\chi^2)^2}, \quad (\text{A3})$$

$$\begin{aligned} D_{11}(p_1, m_\chi, m_a) &\equiv D_{11}[p_1^2, p_1^2, 0, 0, 0, p_1^2; 0, m_\chi^2, 0, m_a^2] - D_{11}[p_1^2, p_1^2, 0, 0, 0, p_1^2; 0, m_\chi^2, m_a^2, m_a^2] \\ &= m_a^2 \frac{(m_a^2 - m_\chi^2)(m_a^2 + 5m_\chi^2) - 2m_\chi^2(2m_a^2 + m_\chi^2) \ln\left(\frac{m_a^2}{m_\chi^2}\right)}{6m_\chi^2(m_a^2 - m_\chi^2)^4}, \end{aligned} \quad (\text{A4})$$

$$\begin{aligned} D_{001}(p_1, m_\chi, m_a) &\equiv D_{001}[p_1^2, p_1^2, 0, 0, 0, p_1^2; 0, m_\chi^2, 0, m_a^2] - D_{001}[p_1^2, p_1^2, 0, 0, 0, p_1^2; 0, m_\chi^2, m_a^2, m_a^2] \\ &= m_a^2 \frac{-2m_a^2 + 2m_\chi^2 + (m_a^2 + m_\chi^2) \ln\left(\frac{m_a^2}{m_\chi^2}\right)}{12(m_a^2 - m_\chi^2)^3}. \end{aligned} \quad (\text{A5})$$

For the two-loop diagrams, the $\Pi_G(\ell^2)$ and $\Pi_{\tilde{G}}(\ell^2)$ in Eq. (7) are

$$\begin{aligned} \Pi_G(\ell^2) &= \sum_{Q=c,b,t} g_Q^2 \left(\frac{m_Q}{v}\right)^2 \int_0^1 dx \left[\frac{\frac{3}{2}x(1-x)}{m_Q^2 - \ell^2 x(1-x)} + m_Q^2 \frac{3x(1-x) + 2(-1-x+x^2)c_{2\theta_q}}{2(m_Q^2 - \ell^2 x(1-x))^2} \right. \\ &\quad \left. - m_Q^4 \frac{1-3x+3x^2 - (1-x)xc_{2\theta_q}}{(m_Q^2 - \ell^2 x(1-x))^3} \right], \end{aligned} \quad (\text{A6})$$

$$\Pi_{\tilde{G}}(\ell^2) = \sum_{Q=c,b,t} g_Q^2 \left(\frac{m_Q}{v}\right)^2 \int_0^1 dx \frac{m_Q^2 s_{2\theta_q}}{(m_Q^2 - \ell^2 x(1-x))^2}. \quad (\text{A7})$$

The $F_G, F_{\tilde{G}}$ functions are

$$\begin{aligned} F_G(p_1^2, m_\chi^2, m_a^2, m_Q^2) &= \int_0^1 dx \left[-\frac{3}{2} \frac{\partial}{\partial m_a^2} X_1\left(p_1^2, m_\chi^2, m_a^2, \frac{m_Q^2}{x(1-x)}\right) \right. \\ &\quad + m_Q^2 \frac{3x(1-x) + 2(-1-x+x^2)c_{2\theta_q}}{2x^2(1-x)^2} \frac{\partial}{\partial m_a^2} X_2\left(p_1^2, m_\chi^2, m_a^2, \frac{m_Q^2}{x(1-x)}\right) \\ &\quad \left. + m_Q^4 \frac{1-3x+3x^2 - x(1-x)c_{2\theta_q}}{x^3(1-x)^3} \frac{\partial}{\partial m_a^2} X_3\left(p_1^2, m_\chi^2, m_a^2, \frac{m_Q^2}{x(1-x)}\right) \right] \end{aligned} \quad (\text{A8})$$

$$F_{\tilde{G}}(p_1^2, m_\chi^2, m_a^2, m_Q^2) = \int_0^1 dx \left[m_Q^2 \frac{s_{2\theta_q}}{x^2(1-x)^2} \frac{\partial}{\partial m_a^2} X_2\left(p_1^2, m_\chi^2, m_a^2, \frac{m_Q^2}{x(1-x)}\right) \right], \quad (\text{A9})$$

where

$$X_1\left(p_1^2, m_\chi^2, m_a^2, \frac{m_Q^2}{x(1-x)}\right) = \frac{1}{m_a^2 - \frac{m_Q^2}{x(1-x)}} \left[B_0(p_1^2, m_a^2, m_\chi^2) - B_0\left(p_1^2, \frac{m_Q^2}{x(1-x)}, m_\chi^2\right) \right], \quad (\text{A10})$$

$$X_2\left(p_1^2, m_\chi^2, m_a^2, \frac{m_Q^2}{x(1-x)}\right) = \frac{1}{m_a^2 - \frac{m_Q^2}{x(1-x)}} \left[X_1\left(p_1^2, m_\chi^2, m_a^2, \frac{m_Q^2}{x(1-x)}\right) - C_0\left(p_1^2, \frac{m_Q^2}{x(1-x)}, m_\chi^2\right) \right], \quad (\text{A11})$$

$$X_3\left(p_1^2, m_\chi^2, m_a^2, \frac{m_Q^2}{x(1-x)}\right) = \frac{1}{m_a^2 - \frac{m_Q^2}{x(1-x)}} \left[X_2\left(p_1^2, m_\chi^2, m_a^2, \frac{m_Q^2}{x(1-x)}\right) - D_0\left(p_1^2, \frac{m_Q^2}{x(1-x)}, m_\chi^2\right) \right], \quad (\text{A12})$$

and

$$\int \frac{d^4\ell}{(2\pi)^4} \frac{1}{[(\ell+p)^2 - M^2](\ell^2 - m^2)} = \frac{i}{(4\pi)^2} B_0(p^2, m^2, M^2), \quad (\text{A13})$$

$$\int \frac{d^4\ell}{(2\pi)^4} \frac{1}{[(\ell+p)^2 - M^2](\ell^2 - m^2)^2} = \frac{i}{(4\pi)^2} C_0(p^2, m^2, M^2), \quad (\text{A14})$$

$$\int \frac{d^4\ell}{(2\pi)^4} \frac{1}{[(\ell+p)^2 - M^2](\ell^2 - m^2)^3} = \frac{i}{(4\pi)^2} D_0(p^2, m^2, M^2). \quad (\text{A15})$$

2. The Passarino-Veltman functions for DM-nucleus scattering

For the elastic scattering $\chi(p_1)q(k_1) \rightarrow \chi(p_2)q(k_2)$, in the zero momentum transfer limit $t \rightarrow 0$, the Passarino-Veltman function is simplified as

$$C_1[p_1^2, (p_1 - p_2)^2, p_2^2; 0, m_a^2, m_a^2] = C_2[p_1^2, (p_1 - p_2)^2, p_2^2; 0, m_a^2, m_a^2] = \frac{(m_\chi^2 - m_a^2) \ln\left(\frac{m_a^2}{m_a^2 - m_\chi^2}\right) + m_\chi^2}{2m_\chi^4}. \quad (\text{A16})$$

The Passarino-Veltman functions for the box diagrams are defined as

$$D_0(p_1, m_\chi, m_a) \equiv D_0[p_1^2, p_1^2, 0, 0, 0, p_1^2; 0, 0, m_a^2, m_a^2] = \frac{\ln\left(1 - \frac{m_a^2}{m_\chi^2}\right)}{m_a^4}, \quad (\text{A17})$$

$$\begin{aligned} D_1(p_1, m_\chi, m_a) &\equiv D_1[p_1^2, p_1^2, 0, 0, 0, p_1^2; 0, 0, m_a^2, m_a^2] \\ &= \frac{(m_a^4 + m_\chi^4) \ln\left(\frac{m_a^2}{m_a^2 - m_\chi^2}\right) - m_\chi^2 \left(m_\chi^2 \ln\left(-\frac{m_a^2}{m_\chi^2}\right) + m_a^2\right)}{2m_a^4 m_\chi^4}, \end{aligned} \quad (\text{A18})$$

$$\begin{aligned} D_{00}(p_1, m_\chi, m_a) &\equiv D_{00}[p_1^2, p_1^2, 0, 0, 0, p_1^2; 0, 0, 0, m_a^2, m_a^2] - D_{00}[p_1^2, p_1^2, 0, 0, 0, p_1^2; 0, 0, m_a^2, m_a^2] \\ &= \frac{(m_a^2 + 2m_\chi^2) \left[m_a^2 m_\chi^2 + (m_a^2 - m_\chi^2)^2 \ln\left(1 - \frac{m_a^2}{m_\chi^2}\right) \right] - m_a^6 \ln\left(-\frac{m_a^2}{m_\chi^2}\right)}{12m_a^4 m_\chi^4} \end{aligned} \quad (\text{A19})$$

$$\begin{aligned} D_{11}(p_1, m_\chi, m_a) &\equiv D_{11}[p_1^2, p_1^2, 0, 0, 0, p_1^2; 0, 0, 0, m_a^2, m_a^2] - D_{11}[p_1^2, p_1^2, 0, 0, 0, p_1^2; 0, 0, m_a^2, m_a^2] \\ &= -\frac{(m_a^6 + 2m_\chi^6) \ln\left(1 - \frac{m_a^2}{m_\chi^2}\right) - m_a^6 \ln\left(-\frac{m_a^2}{m_\chi^2}\right) + m_a^2 m_\chi^2 (m_a^2 + 2m_\chi^2)}{3m_\chi^6 m_a^4} \end{aligned} \quad (\text{A20})$$

$$\begin{aligned} D_{001}(p_1, m_\chi, m_a) &\equiv D_{001}[p_1^2, p_1^2, 0, 0, 0, p_1^2; 0, 0, 0, m_a^2, m_a^2] - D_{001}[p_1^2, p_1^2, 0, 0, 0, p_1^2; 0, 0, m_a^2, m_a^2] \\ &= \frac{1}{24m_a^4 m_\chi^6} \left[2(m_a^2 - m_\chi^2) \left((m_a^6 - m_\chi^6) \ln\left(\frac{m_a^2}{m_a^2 - m_\chi^2}\right) + m_\chi^6 \ln\left(-\frac{m_a^2}{m_\chi^2}\right) \right) \right. \\ &\quad \left. + m_a^2 m_\chi^2 (-2m_a^4 + m_a^2 m_\chi^2 - 2m_\chi^4) \right], \end{aligned} \quad (\text{A21})$$

$$\begin{aligned} D_{111}(p_1, m_\chi, m_a) &\equiv D_{111}[p_1^2, p_1^2, 0, 0, 0, p_1^2; 0, 0, 0, m_a^2, m_a^2] - D_{001}[p_1^2, p_1^2, 0, 0, 0, p_1^2; 0, 0, m_a^2, m_a^2] \\ &= \frac{1}{4m_a^4 m_\chi^8} \left[2(m_a^8 + m_\chi^8) \ln\left(1 - \frac{m_a^2}{m_\chi^2}\right) - 2m_a^8 \ln\left(-\frac{m_a^2}{m_\chi^2}\right) \right. \\ &\quad \left. + m_a^2 m_\chi^2 (2m_a^4 + m_a^2 m_\chi^2 + 2m_\chi^4) \right], \end{aligned} \quad (\text{A22})$$

The $F'_G, F'_\tilde{G}$ functions for the two-loop diagrams are

$$F'_G(p_1^2, m_\chi^2, m_a^2, m_Q^2) = \int_0^1 dx \left[-\frac{3}{2} \frac{\partial}{\partial m_a^2} Y_1 \left(p_1^2, m_\chi^2, m_a^2, \frac{m_Q^2}{x(1-x)} \right) \right. \\ \left. + m_Q^2 \frac{3x(1-x) + 2(-1-x+x^2)c_{2\theta_a}}{2x^2(1-x)^2} \frac{\partial}{\partial m_a^2} Y_2 \left(p_1^2, m_\chi^2, m_a^2, \frac{m_Q^2}{x(1-x)} \right) \right. \\ \left. + m_Q^4 \frac{1-3x+3x^2-x(1-x)c_{2\theta_a}}{x^3(1-x)^3} \frac{\partial}{\partial m_a^2} Y_3 \left(p_1^2, m_\chi^2, m_a^2, \frac{m_Q^2}{x(1-x)} \right) \right] \quad (\text{A23})$$

$$F'_\tilde{G}(p_1^2, m_\chi^2, m_a^2, m_Q^2) = \int_0^1 dx \left[m_Q^2 \frac{s_{2\theta_a}}{x^2(1-x)^2} \frac{\partial}{\partial m_a^2} Y_2 \left(p_1^2, m_\chi^2, m_a^2, \frac{m_Q^2}{x(1-x)} \right) \right], \quad (\text{A24})$$

where

$$Y_1 \left(p_1^2, m_\chi^2, m_a^2, \frac{m_Q^2}{x(1-x)} \right) = \frac{1}{m_a^2 - \frac{m_Q^2}{x(1-x)}} \left[B_1(p_1^2, m_a^2, m_\chi^2) - B_1 \left(p_1^2, \frac{m_Q^2}{x(1-x)}, m_\chi^2 \right) \right], \quad (\text{A25})$$

$$Y_2 \left(p_1^2, m_\chi^2, m_a^2, \frac{m_Q^2}{x(1-x)} \right) = \frac{1}{m_a^2 - \frac{m_Q^2}{x(1-x)}} \left[Y_1 \left(p_1^2, m_\chi^2, m_a^2, \frac{m_Q^2}{x(1-x)} \right) - C_2 \left(p_1^2, \frac{m_Q^2}{x(1-x)}, m_\chi^2 \right) \right], \quad (\text{A26})$$

$$Y_3 \left(p_1^2, m_\chi^2, m_a^2, \frac{m_Q^2}{x(1-x)} \right) = \frac{1}{m_a^2 - \frac{m_Q^2}{x(1-x)}} \left[Y_2 \left(p_1^2, m_\chi^2, m_a^2, \frac{m_Q^2}{x(1-x)} \right) - D_3 \left(p_1^2, \frac{m_Q^2}{x(1-x)}, m_\chi^2 \right) \right], \quad (\text{A27})$$

and

$$\int \frac{d^4 \ell}{(2\pi)^4} \frac{\ell_\mu}{[(\ell+p)^2 - M^2](\ell^2 - m^2)} = \frac{i}{(4\pi)^2} p_\mu B_1(p^2, m^2, M^2), \quad (\text{A28})$$

$$\int \frac{d^4 \ell}{(2\pi)^4} \frac{\ell_\mu}{[(\ell+p)^2 - M^2](\ell^2 - m^2)^2} = \frac{i}{(4\pi)^2} p_\mu C_2(p^2, m^2, M^2), \quad (\text{A29})$$

$$\int \frac{d^4 \ell}{(2\pi)^4} \frac{\ell_\mu}{[(\ell+p)^2 - M^2](\ell^2 - m^2)^3} = \frac{i}{(4\pi)^2} p_\mu D_3(p^2, m^2, M^2), \quad (\text{A30})$$

-
- [1] C. Boehm, M. J. Dolan, and C. McCabe, *JCAP* **08**, 041 (2013), arXiv:1303.6270 [hep-ph].
[2] G. Mangano, A. Melchiorri, P. Serra, A. Cooray, and M. Kamionkowski, *Phys. Rev. D* **74**, 043517 (2006), arXiv:astro-ph/0606190.
[3] C. Boehm, Y. Farzan, T. Hambye, S. Palomares-Ruiz, and S. Pascoli, *Phys. Rev. D* **77**, 043516 (2008), arXiv:hep-ph/0612228.
[4] D. Hooper, M. Kaplinghat, L. E. Strigari, and K. M. Zurek, *Phys. Rev. D* **76**, 103515 (2007), arXiv:0704.2558 [astro-ph].
[5] I. M. Shoemaker, *Phys. Dark Univ.* **2**, 157 (2013), arXiv:1305.1936 [hep-ph].

- [6] O. Balducci, S. Hofmann, and A. Kassiteridis, *Phys. Rev. D* **98**, 023003 (2018), arXiv:1710.09846 [hep-ph].
- [7] M. Chianese, G. Miele, S. Morisi, and E. Peinado, *JCAP* **12**, 016 (2018), arXiv:1808.02486 [hep-ph].
- [8] G.-Y. Huang and N. Nath, *Eur. Phys. J. C* **78**, 922 (2018), arXiv:1809.01111 [hep-ph].
- [9] A. Rajaraman and J. Smolinsky, (2018), arXiv:1811.06619 [hep-ph].
- [10] K. J. Kelly and Y. Zhang, *Phys. Rev. D* **99**, 055034 (2019), arXiv:1901.01259 [hep-ph].
- [11] M. Blennow, E. Fernandez-Martinez, A. Olivares-Del Campo, S. Pascoli, S. Rosauero-Alcaraz, and A. Titov, *Eur. Phys. J. C* **79**, 555 (2019), arXiv:1903.00006 [hep-ph].
- [12] A. Boyarsky, M. Drewes, T. Lasserre, S. Mertens, and O. Ruchayskiy, *Prog. Part. Nucl. Phys.* **104**, 1 (2019), arXiv:1807.07938 [hep-ph].
- [13] K.-Y. Choi, O. Seto, and C. S. Shin, *JHEP* **09**, 068 (2014), arXiv:1406.0228 [hep-ph].
- [14] S. Hannestad, *JCAP* **02**, 011 (2005), arXiv:astro-ph/0411475.
- [15] N. F. Bell, E. Pierpaoli, and K. Sigurdson, *Phys. Rev. D* **73**, 063523 (2006), arXiv:astro-ph/0511410.
- [16] J. F. Beacom, N. F. Bell, and S. Dodelson, *Phys. Rev. Lett.* **93**, 121302 (2004), arXiv:astro-ph/0404585.
- [17] Y. Farzan, M. Lindner, W. Rodejohann, and X.-J. Xu, *JHEP* **05**, 066 (2018), arXiv:1802.05171 [hep-ph].
- [18] V. Brdar, W. Rodejohann, and X.-J. Xu, *JHEP* **12**, 024 (2018), arXiv:1810.03626 [hep-ph].
- [19] W.-F. Chang and J. Liao, (2020), arXiv:2002.10275 [hep-ph].
- [20] N. Hurtado, H. Mir, I. M. Shoemaker, E. Welch, and J. Wyenberg, *Phys. Rev. D* **102**, 015006 (2020), arXiv:2005.13384 [hep-ph].
- [21] J. A. Dror, G. Elor, and R. McGehee, *Phys. Rev. Lett.* **124**, 18 (2020), arXiv:1905.12635 [hep-ph].
- [22] J. A. Dror, G. Elor, and R. McGehee, *JHEP* **02**, 134 (2020), arXiv:1908.10861 [hep-ph].
- [23] D. Z. Freedman, D. N. Schramm, and D. L. Tubbs, *Ann. Rev. Nucl. Part. Sci.* **27**, 167 (1977).
- [24] D. Akimov *et al.* (COHERENT), *Science* **357**, 1123 (2017), arXiv:1708.01294 [nucl-ex].
- [25] M. Drees and M. Nojiri, *Phys. Rev. D* **48**, 3483 (1993), arXiv:hep-ph/9307208.
- [26] J. Hisano, K. Ishiwata, and N. Nagata, *Phys. Rev. D* **82**, 115007 (2010), arXiv:1007.2601 [hep-ph].
- [27] S. Baek, P. Ko, and P. Wu, *JHEP* **10**, 117 (2016), arXiv:1606.00072 [hep-ph].
- [28] S. Baek, P. Ko, and P. Wu, *JCAP* **07**, 008 (2018), arXiv:1709.00697 [hep-ph].
- [29] G. Arcadi, M. Lindner, F. S. Queiroz, W. Rodejohann, and S. Vogl, *JCAP* **03**, 042 (2018), arXiv:1711.02110 [hep-ph].
- [30] T. Li, *Phys. Lett. B* **782**, 497 (2018), arXiv:1804.02120 [hep-ph].
- [31] T. Abe, M. Fujiwara, and J. Hisano, *JHEP* **02**, 028 (2019), arXiv:1810.01039 [hep-ph].
- [32] T. Abe *et al.* (LHC Dark Matter Working Group), *Phys. Dark Univ.* **27**, 100351 (2020), arXiv:1810.09420 [hep-ex].
- [33] T. Li and P. Wu, *Chin. Phys. C* **43**, 113102 (2019), arXiv:1904.03407 [hep-ph].
- [34] K. A. Mohan, D. Sengupta, T. M. Tait, B. Yan, and C.-P. Yuan, *JHEP* **05**, 115 (2019), arXiv:1903.05650 [hep-ph].

- [35] F. Ertas and F. Kahlhoefer, *JHEP* **06**, 052 (2019), [arXiv:1902.11070 \[hep-ph\]](#).
- [36] F. Giacchino, A. Ibarra, L. Lopez Honorez, M. H. G. Tytgat, and S. Wild, *JCAP* **02**, 002 (2016), [arXiv:1511.04452 \[hep-ph\]](#).
- [37] F. Giacchino, L. Lopez-Honorez, and M. H. Tytgat, *JCAP* **08**, 046 (2014), [arXiv:1405.6921 \[hep-ph\]](#).
- [38] A. Ibarra, T. Toma, M. Totzauer, and S. Wild, *Phys. Rev. D* **90**, 043526 (2014), [arXiv:1405.6917 \[hep-ph\]](#).
- [39] S. Colucci, B. Fuks, F. Giacchino, L. Lopez Honorez, M. H. Tytgat, and J. Vandecasteele, *Phys. Rev. D* **98**, 035002 (2018), [arXiv:1804.05068 \[hep-ph\]](#).
- [40] S. Colucci, F. Giacchino, M. H. Tytgat, and J. Vandecasteele, *Phys. Rev. D* **98**, 115029 (2018), [arXiv:1805.10173 \[hep-ph\]](#).
- [41] W. Chao, *JHEP* **11**, 013 (2019), [arXiv:1904.09785 \[hep-ph\]](#).
- [42] X.-G. He, T. Li, X.-Q. Li, J. Tandean, and H.-C. Tsai, *Phys. Rev. D* **79**, 023521 (2009), [arXiv:0811.0658 \[hep-ph\]](#).
- [43] V. Novikov, M. A. Shifman, A. Vainshtein, and V. I. Zakharov, *Fortsch. Phys.* **32**, 585 (1984).
- [44] M. Cirelli, E. Del Nobile, and P. Panci, *JCAP* **10**, 019 (2013), [arXiv:1307.5955 \[hep-ph\]](#).
- [45] F. Bishara, J. Brod, B. Grinstein, and J. Zupan, *JHEP* **11**, 059 (2017), [arXiv:1707.06998 \[hep-ph\]](#).
- [46] G. Aad et al. (ATLAS, CMS), *JHEP* **08**, 045 (2016), [arXiv:1606.02266 \[hep-ex\]](#).
- [47] G. Belanger, F. Boudjema, A. Pukhov, and A. Semenov, *Comput. Phys. Commun.* **180**, 747 (2009), [arXiv:0803.2360 \[hep-ph\]](#).
- [48] G. Belanger, F. Boudjema, A. Goudelis, A. Pukhov, and B. Zaldivar, *Comput. Phys. Commun.* **231**, 173 (2018), [arXiv:1801.03509 \[hep-ph\]](#).
- [49] T. Lin, *PoS* **333**, 009 (2019), [arXiv:1904.07915 \[hep-ph\]](#).
- [50] E. Aprile et al. (XENON), *Phys. Rev. Lett.* **121**, 111302 (2018), [arXiv:1805.12562 \[astro-ph.CO\]](#).
- [51] M. Agostini et al. (Borexino), *JCAP* **02**, 046 (2019), [arXiv:1808.04207 \[hep-ex\]](#).
- [52] F. Petricca et al. (CRESST), *J. Phys. Conf. Ser.* **1342**, 012076 (2020), [arXiv:1711.07692 \[astro-ph.CO\]](#).
- [53] M. J. Dolan, F. Kahlhoefer, C. McCabe, and K. Schmidt-Hoberg, *JHEP* **03**, 171 (2015), [Erratum: *JHEP* **07**, 103 (2015)], [arXiv:1412.5174 \[hep-ph\]](#).
- [54] E. Cortina Gil et al. (NA62), (2020), [arXiv:2007.08218 \[hep-ex\]](#).
- [55] M. B. Wise, *Phys. Lett. B* **103**, 121 (1981).
- [56] H. Leutwyler and M. A. Shifman, *Nucl. Phys. B* **343**, 369 (1990).
- [57] M. Aaboud et al. (ATLAS), *JHEP* **01**, 126 (2018), [arXiv:1711.03301 \[hep-ex\]](#).
- [58] A. M. Sirunyan et al. (CMS), *Phys. Rev. D* **97**, 092005 (2018), [arXiv:1712.02345 \[hep-ex\]](#).
- [59] M. Aaboud et al. (ATLAS), *Eur. Phys. J. C* **78**, 18 (2018), [arXiv:1710.11412 \[hep-ex\]](#).
- [60] M. Aaboud et al. (ATLAS), *JHEP* **06**, 108 (2018), [arXiv:1711.11520 \[hep-ex\]](#).
- [61] V. Khachatryan et al. (CMS), *JHEP* **02**, 135 (2017), [arXiv:1610.09218 \[hep-ex\]](#).